Breakdown of the spin-wave approximation for a Heisenberg ferromagnet

R. S. Fishman
Department of Physics, SU Station Box 5566, North Dakota State University, Fargo North Dakota 58105-5566 and Solid State Division, P.O. Box 2008, Oak Ridge National Laboratory, Oak Ridge, Tennessee 37831*

G. Vignale
Department of Physics and Astronomy, University of Missouri, Columbia, Missouri 65211
(Received 27 September 1990; revised manuscript received 20 December 1990)

By comparing the exact free energy with the free energy of the random-phase approximation (RPA), we find that the spin-wave description of a spin-s Heisenberg ferromagnet breaks down near the temperature $\bar{T}=0.18zJs$, where J is the ferromagnetic coupling constant and z is the number of nearest neighbors. The scaling of the crossover temperature with zJs agrees with the early results of Vaks, Larkin, and Pikin. We calculate this crossover temperature by expanding the RPA free energy in powers of $1/z$ on a d-dimensional hypercubic lattice. While the zeroth- and first-order terms in the RPA expansion agree with the terms in the exact expansion, the second-order term disagrees with the exact $1/z^2$ free energy. Below $\bar{T}$, the difference between the RPA and exact free energies is negligible. So for $T<\bar{T}$, the RPA summation is justified and the spin-wave description is appropriate. Above $\bar{T}$, however, the spin-wave interactions become highly nonlinear and the RPA free energy deviates from the exact result. Because all momentum states contribute to the energy above $\bar{T}$, the transverse free energy enters an equipartition regime and the transverse specific heat tends to zero. As a result, the crossover is marked by a peak in the fluctuation specific heat. The crossover temperature is unchanged if a more sophisticated spin-wave theory is used in place of the RPA. The predicted crossover has been observed as a shoulder in measurements of the total specific heat.

I. INTRODUCTION

The spin-wave approximation[1-3] has been remarkably successful at predicting the low-temperature properties of ferromagnets. Due to this success, many workers[2,4-7] have tried to establish the limitations of the spin-wave approximation for the spin-s Heisenberg model. Even the founders[2-5] of the spin-wave theory expected this approximation to fail above some crossover temperature, when the interactions between the spin waves become nonlinear and the concept of a weakly interacting spin wave loses its meaning. Vaks, Larkin, and Pikin[5] predicted that the spin-wave approximation would fail above a crossover temperature proportional to zJs, where z is the number of nearest neighbors and J is the ferromagnetic coupling constant. They also predicted that the crossover would be marked by an anamoly in the specific heat.

In this paper, we build upon the work of Vaks, Larkin, and Pikin by explicitly calculating the crossover temperature. Our main result is that the crossover temperature occurs very close to $\bar{T}=0.18zJs$, where the fluctuation specific heat of a ferromagnet has a peak.[8] Hence, the crossover leaves a definite thermodynamic signature. In fact, this crossover from a low-temperature spin-wave regime to a high-temperature nonlinear regime has already been observed in measurements of the specific heat. Above the quantum peak in the fluctuation specific heat, the nonlinear spin fluctuations can no longer be described as spin waves. Since the Curie temperature is of order zJs^2, the range of temperatures between $\bar{T}$ and T_C grows as the spin increases. If the temperature is scaled by zJs^2, then the spin-wave regime vanishes in the classical limit of infinite spin.

The fundamental assumption of the spin-wave approximation is that the spin fluctuations can be described as a collection of weakly interacting, particlelike excitations.[4] A single spin wave is, in fact, an exact eigenstate of the Heisenberg Hamiltonian. But due to their interactions, two or more spin waves are not eigenstates.[2] While a state with two spin waves can be diagonalized exactly, states with more than two spin waves are intractable. A simple solution to this dilemma, popularized by Dyson,[2] is to simply ignore the many-body interactions between three or more spin waves. The ferromagnetic Hamiltonian is then replaced by a spin-wave Hamiltonian which is fourth order in the spin-wave creation and annihilation operators and which couples only two spin waves at once. This approximation is justified if the number of spin waves is small so that many-body interactions are unlikely. As the temperature increases, however, the number of spin waves grows and many-body interactions become more common.

Another weakness of the spin-wave picture is that it violates the spin kinematics.[2,4] A proper treatment of the spin kinematics restricts the eigenvalues of the spin operator S_{iz} on site i to quantized values between s and $-s$. Since the ground state is defined with $S_{iz}=s$ at every site, only $2s$ spin deviations are permitted at each lattice site. Without introducing an awkward set of projection operators, the spin-wave approximation cannot enforce

these kinematic constraints. Since the average number of spin deviations is small at low temperatures, the kinematic constraints are customarily ignored[4] by the spin-wave approximation. Because the spin operators are replaced by a set of Bose operators with particlelike properties, the number of spin deviations at each site can assume any integer value between 0 and ∞. Hence, the spin-wave approximation will violate the kinematic constraints when the number of spin deviations exceeds $2s$.

The interactions between spin waves are usually investigated in a perturbative expansion about a noninteracting spin-wave Hamiltonian. In the $1/s$ expansion of Holstein and Primakoff,[9] the spin-wave interactions are contained in a $1/s$ correction to the noninteracting Hamiltonian. In the random-phase approximation[10,11] (RPA), the single-particle energies are renormalized by the presence of other spin waves at finite temperatures. The renormalized spin waves form the basis set of noninteracting particles at any temperature. More complex spin-wave interactions will couple these renormalized excitations. Any such perturbative approach breaks down when the single-particle excitations form bound states.[4] Dyson[2] demonstrated that two spin waves cannot form a bound state if their total momentum $\mathbf{K}$ is sufficiently small. But Wortis[4] showed that if $\mathbf{K}$ is close to the edge of the Brillouin zone, two spin waves can form a bound state[4] with energy of order zJs. Above the crossover temperature $\overline{T} \propto zJs$, the formation of bound states invalidates the spin-wave approximation.

This crossover affects the thermodynamics of a ferromagnet. For example, at low temperatures the exact free energy of a ferromagnet can be expanded in powers of $T^{1/2}$. In three dimensions, the lowest-order term in the transverse free energy is of order $T^{5/2}$. Because the exact free energy also contains exponential corrections, proportional to powers of $e^{-J/T}$, the power-series expansion is only asymptotically correct. Dyson[2] conjectured that the spin-wave description remains valid only so long as the exponential corrections can be neglected and the power-series expansion is meaningful. In this paper, we find that the largest exponential correction to the power-series expansion is proportional to some power of $e^{-zJs/T}$. So above a temperature of order zJs, both the analytic and nonanalytic terms in the free energy are equally important. Just as argued by Dyson, the breakdown of the spin-wave picture coincides with the failure of the asymptotic expansion.

In the nonlinear regime above $\overline{T}$, all of the many-body interactions contribute to the free energy. These many-body interactions depend very sensitively on the kinematic constraints discussed above. Unlike spin waves, the nonlinear fluctuations above $\overline{T}$ are more easily described in real space, with the kinematic constraints automatically enforced. A convenient real-space formalism for cataloging the many-body interactions and studying their effects is the $1/z$ expansion.[8,12] Any thermodynamic quantity, such as the order parameter or free energy, may be expanded in powers of $1/z$. The lowest-order term in such an expansion agrees with mean-field (MF) theory, which neglects the correlation of fluctuations on different lattice sites. The higher-order $1/z$ corrections embody the coupling of spin fluctuations on neighboring sites.

Because the $1/z$ expansion is formally exact, it can be used to check the accuracy of approximate techniques, order by order in $1/z$. Since even the spin-wave Hamiltonian proposed by Dyson cannot be treated exactly, we use the RPA to represent the more general class of spin-wave theories. While we recognize that the RPA has some serious weaknesses, our calculation of the crossover temperature is independent of the particular spin-wave theory chosen. The relative simplicity of the RPA enables us to clearly demonstrate the reasons for the failure of the spin-wave picture.

To calculate the crossover temperature, we compare the $1/z$ expansion of the exact free energy with the $1/z$ expansion of the RPA free energy. As shown in Sec. III, the RPA free energy can be expressed as an infinite series of ring diagrams, with escalating order in $1/z$. To zeroth and first order in $1/z$, the RPA free energy is exact. But to second order in $1/z$, the RPA free energy disagrees with the exact result,[13] calculated on a d-dimensional hypercubic lattice with $z=2d$ nearest neighbors. The ring diagram that represents the second-order RPA free energy is only one of the infinitely many diagrams which contribute to the $1/z^2$ correction to the exact free energy.

Above the temperature $T_z \propto Js$ but not too close to the Curie temperature, the $1/z$ expansion of the RPA free energy converges rapidly. By comparing the RPA and exact free energies, we find that the spin-wave approximation remains valid up to the crossover temperature $\overline{T} \approx 0.18zJs > T_z$. Below $\overline{T}$, the RPA and exact free energies are approximately equal. Hence, the summation over ring diagrams is probably justified and the spin-wave description is appropriate. Above $\overline{T}$, however, the RPA and exact free energies begin to differ significantly and the spin-wave picture breaks down.

Of course, the RPA can be improved by including interactions between the renormalized excitations. But this procedure will, at best, only incrementally increase the crossover temperature. The spin-wave free energy will still deviate from the exact free energy at a temperature very close to $\overline{T}$. Yet such refinements will certainly improve the spin-wave approximation below the crossover temperature, where the spin waves are well defined.

Although the crossover temperature may lie slightly above or below the peak in the fluctuation specific heat, we shall usually not distinguish between the two. The quantum peak at $\overline{T}$ appears in the first-order specific heat C_1/N, which is the same for the RPA and the $1/z$ expansion. We show in Sec. III that the quantum peak in C_1/N survives the summation over ring diagrams to appear in the total RPA fluctuation specific heat. Hence, the quantum peak appears in calculations on both sides of the crossover. A shoulder in the total specific heat signals the crossover between the linear and nonlinear regimes.

The crossover is most easily explained in terms of the spin-wave interactions. At low temperatures, the maximum spin-wave frequency is $2zJs$. Above $\overline{T} \propto zJs$, the transverse spin-wave free energy enters an equipartition region in which all spin wave states contribute to the energy. The interactions between spin waves with large

momenta are highly nonlinear and so the spin fluctuations above $\bar{T}$ can no longer be described as weakly interacting, long-wavelength excitations. Because the transverse free energy becomes a linear function of T above $\bar{T}$, the transverse, fluctuation specific heat peaks at the crossover temperature.

This paper is divided into five main sections. In Sec. II we review the $1/z$ expansion and calculate the $1/z^2$ correction to the free energy. By summing over ring diagrams in Sec. III, we demonstrate that the RPA free energy is exact only up to first order in $1/z$. Using this free energy, we numerically evaluate the RPA fluctuation specific heat. The main results of this paper are presented in Sec. IV, in which we compare the exact and RPA free energies through second order in $1/z$. In this section, we also evaluate the second-order, fluctuation specific heat. Finally, in Sec. V we consider a more general class of spin-wave theories. The physical significance and observability of the crossover is also discussed.

Technical details that would clutter the main text are relegated to the Appendixes. Appendix A contains a proof of the semi-invariant expansion used to evaluate the $1/z$ expansion of the free energy; Appendix B contains the results for the $1/z$ and $1/z^2$ corrections to the exact and RPA free energies; Appendix C demonstrates that the entropy and free energy of the $1/z$ expansion are continuous at the Curie temperature, as required for a second-order phase transition; and Appendix D provides an alternate derivation of the RPA based on linear-response theory.

II. THE $1/z$ EXPANSION

The $1/z$ expansion for a Heisenberg ferromagnet was originally formulated by Horwitz and Callen,[14] Stinchcombe,[11] Brout,[15] and Vaks, Larkin, and Pikin.[5] Its development was interrupted by the discovery of "anomalies" in the $1/z$ corrections to the order parameter and free energy at the MF Curie temperature. Recently, Fishman and Liu[8] (FL) have established that these so-called "anomalies" are required for the consistency of the theory and lead to no unphysical effects. For example, the divergence of the $1/z$ correction to the order parameter at the MF Curie temperature signals a shift in the Curie temperature from the MF value. As discussed below, the other "anomalies" of the $1/z$ expansion in zero field are also simple to understand.

In this section, we extend the discussion of FL to calculate the $1/z^2$ corrections to the free energy. Our starting point is the Hamiltonian for a spin-s Heisenberg model with N lattice sites:

$$H=-J\sum_{\langle i,j\rangle}\mathbf{S}_i\cdot\mathbf{S}_j\ , \tag{1}$$

where $J>0$ is the exchange coupling and the spin operators obey the commutation relations

$$[S_{i\alpha},S_{j\beta}]=-i\delta_{ij}\epsilon_{\alpha\beta\gamma}S_{i\gamma} \tag{2}$$

with $\hbar=1$. As in FL, we separate H into a MF term $H_{\rm eff}$, a constant term H_1, and a fluctuation term H_2:

$$H=H_{\rm eff}+H_1+H_2\ , \tag{3}$$

$$H_{\rm eff}=-zJM_0\sum_i S_{iz}\ , \tag{4}$$

$$H_1=\tfrac{1}{2}NzJM_0^2\ , \tag{5}$$

$$H_2=-J\sum_{\langle i,j\rangle}R_{ij}\ , \tag{6}$$

$$R_{ij}=(S_{iz}-M_0)(S_{jz}-M_0)+S_{ix}S_{jx}+S_{iy}S_{jy}\ , \tag{7}$$

where $M_0=\langle S_{1z}\rangle_{\rm MF}$ is the MF order parameter. The MF expectation value of any operator A is evaluated by neglecting H_2 and ignoring the c-number H_1:

$$\langle A\rangle_{\rm MF}=\frac{1}{Z_0}{\rm Tr}(e^{-\beta H_{\rm eff}}A)\ , \tag{8}$$

$$Z_0={\rm Tr}(e^{-\beta H_{\rm eff}})\ . \tag{9}$$

Notice that $\langle A\rangle_{\rm MF}$ depends only on the dimensionless temperature $T^*=T/zJ$ and on the spin s.

The MF theory of the Heisenberg model is well known.[1] Because $H_{\rm eff}$ is the sum of single-site operators, the MF partition function $Z_0=Z_{00}^N$ is the product of the single-site partition functions

$$Z_{00}=\frac{\sinh[\beta^*M_0(s+\frac{1}{2})]}{\sinh(\beta^*M_0/2)} \tag{10}$$

with $\beta^*=1/T^*$. Using Eqs. (8)–(10), we find that the MF order parameter M_0 is the solution of the self-consistent equation

$$M_0=(s+\tfrac{1}{2})\coth[\beta^*M_0(s+\tfrac{1}{2})]-\tfrac{1}{2}\coth(\tfrac{1}{2}\beta^*M_0)\ . \tag{11}$$

Upon setting $M_0(T^*)$ to zero, we obtain the MF Curie temperature $T_C^*=s(s+1)/3$. Explicitly including the contribution of H_1, the MF free energy is

$$\frac{F_0}{NzJ}=-T^*\ln Z_0+\tfrac{1}{2}M_0^2\ , \tag{12}$$

which is a function only of T^* and s.

In terms of F_0/NzJ, the MF specific heat is given by

$$\frac{C_0(T^*)}{N}=-T^*\frac{d^2}{dT^{*2}}\frac{F_0}{NzJ}\ . \tag{13}$$

As required by Nernst's theorem for any finite value of the spin, C_0/N vanishes at $T^\dagger\equiv T^*/s(s+1)=0$. But in the classical limit $s\to\infty$, C_0/N approaches 1 at $T^\dagger=0$. Therefore, the MF specific heat develops a shoulder as the spin increases. For $s\geq 3$, $C_0/NT^\dagger$ contains a peak below the Curie temperature. Both features are caused by the exponential term e^{-M_0/T^*} in the MF specific heat. As discussed below, the shoulder in C_0/N and the peak in $C_0/NT^\dagger$ occur very close to the crossover temperature $\bar{T}$.

Of course, MF theory neglects the correlation of fluctuations on neighboring sites, which are introduced by the fluctuation Hamiltonian H_2. In the formal limit $z\to\infty$ (only possible in infinite dimension), the mean-field zJ experienced by every spin diverges and the coupling of

fluctuations can be ignored. But as the coordination number decreases, the coupling of fluctuations on neighboring sites becomes increasingly important. Hence, the effects of correlations can be investigated with a $1/z$ expansion about MF theory. In the $1/z$ correction to MF theory, the spin correlations follow simple, nonintersecting paths in the lattice. For example, the $1/z$ correction to the MF free energy involves the spin correlations between two neighboring sites. As the order of the correction increases, the correlations follow more complicated paths.

Unlike a cluster expansion, the $1/z$ expansion does *not* restrict the fluctuations to some finite cluster of sites in the lattice. For example, the $1/z$ correction to the order parameter[8] and the $1/z^2$ correction to the free energy, calculated below, involve an infinite number of lattice sites. Although higher-order corrections become increasingly more difficult to calculate, every term in the $1/z$ expansion can be evaluated exactly. The two lowest-order terms in the $1/z$ expansion are independent of the topology of the lattice: they are functions only of the coordination number z, not of the lattice dimension d. Starting with the second-order correction, the fluctuation corrections also depend on the lattice dimension.

Any expectation value can be expanded in powers of $1/z$. Formally, the expansion of the order parameter $M=\langle S_{1z}\rangle$ can be written

$$M=M_0(T^*)+\frac{1}{z}M_1(T^*)+\frac{1}{z^2}M_2(T^*)+\cdots , \tag{14}$$

where every coefficient M_i is a function only of the dimensionless temperature T^* and of the spin s. Diagrammatically, the first-order correction M_1 is represented by the infinite set of terms shown in Fig. 1. Each line represents a factor of JR_{ij} which couples neighboring sites. It is straightforward to evaluate the order of each diagram in Fig. 1. For example, the diagram $M_1^{(2)}$ couples site 1 with any of the z neighboring sites j. Since each line carries a factor of J, this diagram is of order $zJ^2=(zJ)^2/z$. Because all factors of zJ combine with β to yield the dimensionless parameter β^*, diagram $M_1^{(2)}$ is of order $1/z$. Similar counting arguments demonstrate that the mth-order diagram $M_1^{(m>2)}/z$ is also of order $1/z$.

As shown in FL, the sum over diagrams $M_1^{(m>2)}/z$ can be evaluated exactly:

$$M_1(T^*)=\sum_{m=2}^{\infty}M_1^{(m)}(T^*)=\frac{M_1^{(2)}(T^*)}{1-f(T^*)} , \tag{15}$$

where

$$M_1^{(2)}=\tfrac{1}{2}\beta^{*2}\langle R_{12}^2(S_{1z}-M_0)\rangle_{\rm MF} . \tag{16}$$

The function f is given by

$$f=\beta^*\langle(S_{1z}-M_0)^2\rangle_{\rm MF} , \tag{17}$$

which is equivalent to the bare susceptibility in a uniform magnetic field.

Because M_1 is negative, the coupling of fluctuations suppresses the long-order of the spins. As T^* approaches the MF Curie temperature, f approaches 1 and M_1 diverges to $-\infty$. This divergence signals a shift in T_C^* from the MF value $T_0\equiv s(s+1)/3$. Like the order parameter, the Curie temperature can also be expanded in powers of $1/z$:

$$T_C^*=T_0+\frac{1}{z}T_1+\frac{1}{z^2}T_2+\cdots . \tag{18}$$

The first-order correction T_1 is derived by expanding the condition $M(T_C^*)=0$ to first order in $1/z$, with the result

$$T_1=-\tfrac{1}{3}s(s+1)-\tfrac{1}{4} . \tag{19}$$

In the limit of large s, both T_1 and T_0 are proportional to s^2. The second-order corrections M_2 and T_2 will be derived elsewhere.

Two equivalent methods may be used to calculate the fluctuation corrections to the MF free energy. The first and more straightforward method is to directly expand the partition function in powers of H_2:

$$Z=\sum_{n=0}^{\infty}(-1)^n\beta^n\frac{1}{n!}{\rm Tr}[e^{-\beta H_{\rm eff}}(H_2)^n] . \tag{20}$$

Each term in the partition function is represented by a diagram without free ends. After scaling the temperature by zJ, we identify and collect all the diagrams of a particular order in $1/z$. The lowest-order term in the $1/z$ expansion is the MF partition function Z_0. Higher-order corrections are proportional to powers of N: a connected diagram is proportional to N while a nonconnected diagram with $m\geq 2$ parts is proportional to N^m.

To eliminate these extensive terms, the partition function is rewritten as an intensive quantity exponentiated to the Nth power:

$$Z=\left[\sum_{n=0}^{\infty}\frac{1}{z^n}Q_n\right]^N . \tag{21}$$

Through second order in $1/z$, the coefficients Q_i are

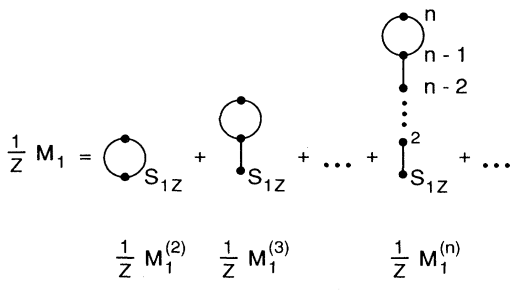

FIG. 1. Diagrammatic representation of the first-order corrections to the order parameter.

$$Q_0 = Z_{00} \ , \tag{22}$$

$$\frac{Q_1}{Q_0} = \tfrac{1}{4}\beta^{*2}\langle R_{12}^2 \rangle_{\rm MF} \ , \tag{23}$$

$$\begin{aligned}\frac{Q_2}{Q_0} = {} & \tfrac{1}{192}\beta^{*4}\langle P(R_{12}R_{23}R_{34}R_{41})\rangle_{\rm MF} + \tfrac{1}{12}\beta^{*3}\langle R_{12}^3 \rangle_{\rm MF} \\ & + \tfrac{1}{48}\beta^{*4}\langle P(R_{12}^2 R_{23}^2)\rangle_{\rm MF} - \tfrac{3}{32}\beta^{*4}\langle R_{12}^2 \rangle_{\rm MF}^2 \\ & - \frac{1}{2\times 5!}\beta^{*5}\langle P(R_{12}^2 R_{23}R_{34}^2)\rangle_{\rm MF} \\ & - \frac{1}{2\times 6!}\beta^{*6}\langle P(R_{12}^2 R_{23}R_{34}R_{45}^2)\rangle_{\rm MF} - \cdots \ . \end{aligned} \tag{24}$$

Unlike Q_0 and Q_1, Q_2 contains an infinite number of terms. The permutation operator P simply sums all distinct permutations of the R_{ij} operators. For example,

$$\begin{aligned}\langle P(R_{12}^2 R_{23}^2)\rangle_{\rm MF} = {} & \langle R_{12}(R_{12}R_{23}^2 + R_{23}R_{12}R_{23} \\ & + R_{23}^2 R_{12})\rangle_{\rm MF} \\ & + \langle R_{23}(R_{23}R_{12}^2 + R_{12}R_{23}R_{12} \\ & + R_{12}^2 R_{23})\rangle_{\rm MF} \ . \end{aligned} \tag{25}$$

Because the various R_{ij} do not commute, the MF expectation value of each permutation must be evaluated separately.

The partition function can now be related to the free energy, which is also expanded in powers of $1/z$ as

$$\frac{F}{NzJ} = \frac{F_0}{NzJ} + \frac{1}{z}\frac{F_1}{NzJ} + \frac{1}{z^2}\frac{F_2}{NzJ} + \cdots \ , \tag{26}$$

where every coefficient F_i/NzJ is a function only of T^* and s. After some simple algebraic manipulation, we find that

$$\frac{F_0}{NzJ} = -T^* \ln Q_0 + \tfrac{1}{2}M_0^2 \ , \tag{27}$$

$$\frac{F_1}{NzJ} = -T^* \frac{Q_1}{Q_0} \ , \tag{28}$$

$$\frac{F_2}{NzJ} = -T^* \frac{Q_2}{Q_0} + \frac{1}{2}T^* \left[\frac{Q_1}{Q_0}\right]^2 . \tag{29}$$

Of course, Eq. (27) for F_0/NzJ is equivalent to Eq. (12) above.

The fluctuation free energy is represented diagrammatically in Fig. 2. As discussed earlier, simple counting arguments can be used to evaluate the order of any diagram. For example, the one-loop diagram which represents F_1/NzJ can occupy $Nz/2$ positions between neighboring sites. So the contribution of this diagram is proportional to $zJ^2 = (zJ)^2/z$ or, in dimensionless units, to $1/z$. Similarly, the diagrams which represent F_2/NzJ are all of order $1/z^2$. Like the diagrams $F_2^{(m\geq 5)}/NzJ$, the diagram $F_2^{(b)}/NzJ$ and the ("two-loop") diagram $F_2^{(c)}/NzJ$ do not depend on the dimension of the lattice. But as discussed below, the square diagram $F_2^{(a)}/NzJ$ does depend on the lattice topology. This ring diagram can occupy $Nd(d-1)/2$ different positions in a hypercubic lattice of dimension d. Using the relation $z = 2d$, we find that its contribution is proportional to $z^2J^4 = (zJ)^4/z^2$.

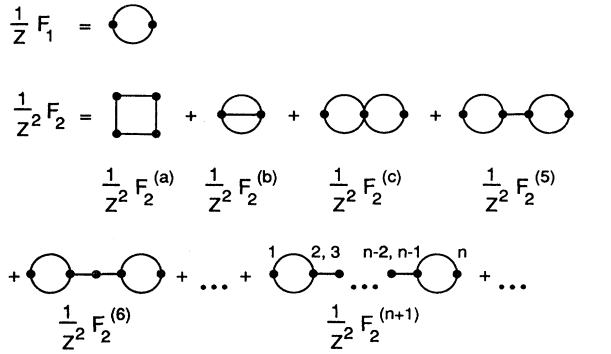

FIG. 2. Diagrammatic representation of the first- and second-order corrections to the free energy.

While the other diagrams each correspond to a single term in F_2/NzJ, the two-loop diagram corresponds to *two* terms in the fluctuation free energy: the connected term $\langle R_{12}^2 R_{23}^2 \rangle_{\rm MF}$ as well as the disconnected term $\langle R_{12}^2 \rangle_{\rm MF}^2$. The disconnected term is produced when $F_2^{(c)}/NzJ$ is cut along its central vertex to create two one-loop diagrams. If such a procedure were performed on any of the other diagrams, the disconnected parts would not survive.

Notice that the diagrams which represent F_2/NzJ involve the many-body interactions between three or more spin fluctuations at the same lattice site. For example, the diagrams $F_2^{(m\geq 5)}/NzJ$ and $F_2^{(b)}/NzJ$ contain vertices where three fluctuations interact at once. In the two-loop diagram, four spin fluctuations interact at the central site. Generally, the complexity of the many-body interactions increases with the order of the correction. In addition to the three- and four-body interactions contained in F_2/NzJ, the third-order free energy F_3/NzJ also involves five- and six-body interactions.

An alternate and somewhat more elegant method of deriving the fluctuation free energy $\Delta F = F - F_0$ is to directly expand ΔF in terms of semi-invariants. This method was originally developed by Horwitz and Callen[14] to evaluate the free energy of the Ising model. The semi-invariant expansion for the Heisenberg model is derived in Appendix A, where we show that

$$\Delta F = -T \ln\langle e^{-\beta H_2}\rangle_{\rm MF} \ , \tag{30}$$

may be expressed as

$$\Delta F = -T \sum_{n=1}^{\infty} \frac{(\beta J)^n}{n!} \prod_{\alpha=1}^{n} \sum_{\langle i_\alpha, j_\alpha \rangle} M^{(n)}_{\{i_1,j_1;\ldots;i_n,j_n\}} \ . \tag{31}$$

Here, $M^{(n)}_{\{i,j\}}$ is the semi-invariant of order n, which subtracts off parts of a diagram in a very specific fashion. For example,

$$M_{12}^{(1)} = \langle R_{12} \rangle_{\mathrm{MF}} , \tag{32}$$

$$M_{1,2;1,2}^{(2)} = \langle R_{12}^2 \rangle_{\mathrm{MF}} - \langle R_{12} \rangle_{\mathrm{MF}}^2 = \langle R_{12}^2 \rangle_{\mathrm{MF}} , \tag{33}$$

$$M_{1,2;1,2;2,3;2,3}^{(4)} = \langle R_{12}^2 R_{23}^2 \rangle_{\mathrm{MF}} - \langle R_{23}^2 \rangle_{\mathrm{MF}} \langle R_{12}^2 \rangle_{\mathrm{MF}} . \tag{34}$$

As mentioned earlier, the extra term in Eq. (34) corresponds to the two one-loop diagrams that are created when the two-loop diagram is cut along its central vertex. Since the disconnected parts of any other $1/z^2$ diagram cannot survive on their own, only $F_2^{(c)}/NzJ$ contains an extra contribution from the semi-invariant method.

In the semi-invariant expansion of Eq. (31), disconnected diagrams appear only as corrections to connected diagrams. Hence, Eq. (31) is similar to the linked-cluster expansion,[16] which eliminates disconnected diagrams from the expansion of the free energy. Unlike the linked-cluster expansion, however, the semi-invariant expansion is valid even without a Wick's theorem for the spin operators. The summation over nearest neighbors in Eq. (31) automatically performs the permutation P over all possible arrangements of the operators R_{ij}. Not surprisingly, the semi-invariant summation agrees with the direct expansion of the partition function in Eqs. (26)–(28).

We complete this formal discussion by expanding the specific heat C/N in powers of $1/z$ as

$$\frac{C}{N} = \frac{C_0}{N} + \frac{1}{z}\frac{C_1}{N} + \frac{1}{z^2}\frac{C_2}{N} + \cdots , \tag{35}$$

where C_0/N is the MF specific heat discussed earlier. The coefficients in this expansion are related to the free-energy parameters by

$$\frac{C_n(T^*)}{N} = -T^* \frac{d^2}{dT^{*2}} \frac{F_n}{NzJ} , \tag{36}$$

for all $n \geq 0$.

The first-order corrections to the MF free energy and specific heat were calculated in FL. Unlike M_1, which involves an infinite number of diagrams, F_1/NzJ involves only the one-loop diagram. The expression for F_1/NzJ is reproduced in Appendix B while the first-order fluctuation specific heat, obtained by numerical differentiation of the free energy, is plotted in Fig. 3. Remarkably, C_1/N contains a peak below T_0 at the temperature $\bar{T}^*$. In Sec. IV, we show that the temperature $\bar{T}^*$ of the peak is approximately equal to $0.177s$ or that

$$\bar{T}^\dagger \equiv \bar{T}^*/s(s+1) \approx 0.177/(s+1) .$$

As mentioned earlier, this peak signals the breakdown of the spin-wave approximation. When $s = \frac{1}{2}$, the peak is hidden by the large fluctuation specific heat near the Curie temperature. The peak first appears when $s = 1$. With the specific heat plotted versus $T^\dagger$ in Fig. 3, the peak disappears in the classical limit of infinite spin.

We emphasize that the peak is a quantum-mechanical phenomenon induced by the noncommutation of the transverse and longitudinal spin components. Since the transverse components are absent in the Ising model, the fluctuation specific heat of that model does not contain a peak.[8]

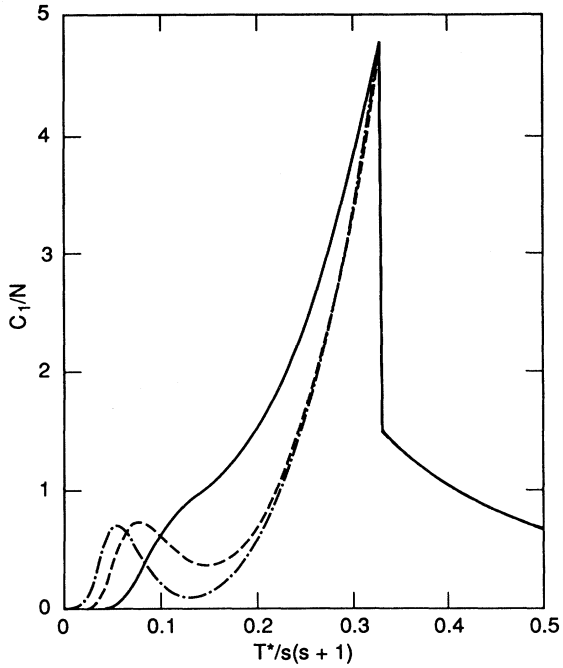

FIG. 3. The first-order, fluctuation specific heat for $s = \frac{1}{2}$ (solid), $\frac{3}{2}$ (long dashed), and $\frac{5}{2}$ (short dashed).

Because the diagrams which represent M_1 and F_1/NzJ do not contain closed paths, the first-order corrections calculated in FL are *independent* of the topology or dimension of the lattice. For instance, T_1/z is the same for a hexagonal lattice in two dimensions or a cubic lattice in three dimensions. But the $1/z^2$ corrections to the order parameter and free energy do involve diagrams with closed paths, such as the square diagram in Fig. 2. So the second-order corrections depend on the topology of the lattice. For example, the square diagram will contribute to the $1/z^2$ free energy in a cubic lattice but not in a hexagonal lattice, even though both have $z = 6$ nearest neighbors.

A particularly important class of closed-path diagrams are the ring diagrams, such as the one-loop and square diagrams of Fig. 2. Previous authors[8,11,15] have assumed that every ring diagram is of order $1/z$. Since the contribution of a ring diagram with $n > 2$ lines depends on the topology of the lattice, they were classified by FL as the *lattice-dependent* corrections of order $1/z$. But in the next section, we show that the contribution of a ring diagram with $2n$ lines (a ring diagram with an odd number of lines is prohibited on a hypercubic lattice) is of order $1/z^n$, not of order $1/z$ as previously assumed. In Sec. IV, we use this result to expand the RPA free energy in powers of $1/z$.

Unlike F_1/NzJ, the second-order correction F_2/NzJ contains an infinite number of terms. Using our previous results, the infinite sum over the diagrams $F_2^{(m \geq 5)}/NzJ$ can be evaluated exactly. Each such diagram is simply

the product of a diagram $M_1^{(m-3)}$ and a diagram $M_1^{(2)}$:

$$\frac{F_2^{(m)}}{NzJ} = -\tfrac{1}{2} M_1^{(m-3)} M_1^{(2)}, \quad \text{with } m \geq 5 . \tag{37}$$

Summing over m, we find that the total contribution of all diagrams $F_2^{(m \geq 5)}/NzJ$ is

$$\sum_{m=5}^{\infty} \frac{F_2^{(m)}}{NzJ} = -\frac{1}{2} \frac{(M_1^{(2)})^2}{1-f} . \tag{38}$$

Unlike M_1, this function approaches a finite value at the MF Curie temperature. Because the right-hand side of Eq. (38) vanishes above T_0, F_2/NzJ is discontinuous at T_0. This "anomaly" is discussed below. The final result for F_2/NzJ, presented in Appendix B, depends on the MF order parameter $M_0(T^*)$ and the functions

$$G_n(T^*) = \langle S_{1z}^{n+1} \rangle_{\rm MF} = \frac{1}{Z_{00}} \sum_{m=-s}^{s} m^{n+1} e^{\beta^* m M_0} , \tag{39}$$

$$Z_{00} = \sum_{m=-s}^{s} e^{\beta^* m M_0} , \tag{40}$$

with $n = 1$, 2, or 3. The single-site MF partition function Z_{00} was explicitly evaluated in Eq. (10). Of course, $G_0(T^*) = M_0(T^*)$.

Our results for the free energy are somewhat complicated. As required for the consistency of the expansion, both F_1/NzJ and F_2/NzJ vanish at $T^* = 0$. At low temperatures, each correction to the free energy can be expanded in powers of

$$y = e^{-M_0(T^*)/T^*} \approx e^{-s/T^*} , \tag{41}$$

which vanishes as T^*/s tends to zero. For $s < \infty$, the low-temperature expansions of the MF and fluctuation free energies are given by

$$\frac{F_0}{NzJ} = -\tfrac{1}{2} s^2 - T^* y + \tfrac{1}{2} y^2 (1 - T^*) + O(y^3) , \tag{42}$$

$$\frac{F_1}{NzJ} = -\tfrac{1}{4} \beta^* y [2s^2 + (2s-1)^2 y] + O(y^3) , \tag{43}$$

$$\begin{aligned} \frac{F_2}{NzJ} = & -\tfrac{1}{8} \beta^{*3} s^2 y [s^2 + 2y(2s-1)^2] \\ & - \tfrac{1}{12} \beta^{*2} y^2 (1 - 6s + 6s^2) \\ & - \tfrac{1}{8} \beta^{*4} s^4 y^2 + O(y^3) . \end{aligned} \tag{44}$$

These analytic results are used in Sec. IV to compare the RPA and exact free energies.

For $s = \frac{3}{2}$, the numerical results for F_2/NzJ are shown in the solid curve of Fig. 4. Both F_2/NzJ and its slope change discontinuously at the MF Curie temperature. Although F_1/NzJ is continuous at T_0, the first-order entropy S_1/N is discontinuous at T_0. Despite appearances, however, neither the total free energy F/NzJ nor the total entropy S/N are discontinuous at the true Curie temperature $T_C^* < T_0$. Above T_C^*, the free energy and entropy should be evaluated with M_0 set to zero in Eqs. (3)–(7). Below T_C^*, the corrections to the free energy and entropy are properly evaluated with $M_0 > 0$. So to calculate the change in the free energy or entropy across the Curie temperature, the shift in the Curie temperature must be carefully observed. In Appendix C, we show that *the discontinuities of F_2/NzJ and S_1/N at T_0 are required for the continuity of the total free energy and entropy at T_C^**. Like the divergence of M_1 at T_0, the discontinuities in F_2/NzJ, S_1/N, and S_2/N signal the shift in the Curie temperature from the MF value.

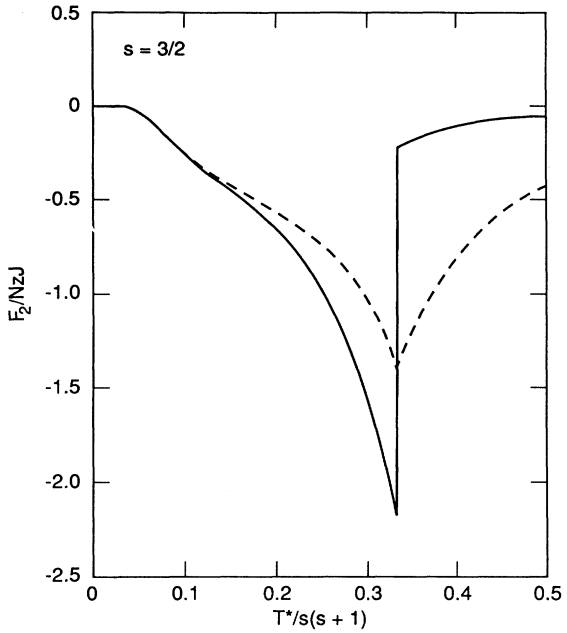

FIG. 4. The second-order free energies F_2/NzJ (solid) and $F_2^{\rm RPA}/NzJ$ (dashed) for $s = \frac{3}{2}$.

The results for the second-order specific heat C_2/N will be presented in Sec. IV. Both C_1/N and C_2/N behave like $e^{-\beta^* s}$ at low temperatures. This result disagrees with the measurement[1] of a $T^{3/2}$ specific heat at low temperatures in a three-dimensional ferromagnet. In the following section, we show that the $T^{3/2}$ specific heat is recovered when the infinite number of ring diagrams are summed in a special way. Below $\bar{T}$, this summation is justified and the spin-wave thermodynamics is accurate.

Despite the advantages of the $1/z$ expansion, it also has some serious weaknesses. The absence of spin-wave thermodynamics at low temperatures is certainly the most significant. In two-dimensional ferromagnets, spin waves destroy the long-range order of the spins.[1] Since any finite expansion in powers of $1/z$ does not obey the Mermin-Wagner theorem, this method cannot be applied to two-dimensional systems. Although we use a formal expansion in $1/z$ to study the class of hypercubic lattices with $z = 2d$ nearest neighbors, our results are strictly relevant only to three-dimensional ferromagnets.

The $1/z$ expansion has other shortcomings near the Curie temperature. Although the critical exponents of MF theory are only correct in four dimensions and higher, the critical exponents of the $1/z$ expansion are unchanged from the MF exponents. The $1/z$ expansion

also yields a finite specific heat at T_C. Since the Curie temperature itself is shifted by fluctuation corrections, the $1/z$ expansion does not break down near T_C. Rather, these shortcomings imply that the critical exponents and the specific heat near T_C are nonanalytic functions of $1/z$.

III. THE RANDOM-PHASE APPROXIMATION

The RPA is a method which linearizes the spin fluctuations about the MF order parameter.[10] A simple derivation of the RPA based on linear-response theory is given in Appendix D. In contrast to the $1/z$ expansion, the RPA sums diagrams of all orders in $1/z$ in an uncontrolled fashion. Although the RPA is exact up to first order in $1/z$, it is only approximate above that order. The main merit of the RPA is that it yields the familiar spin-wave thermodynamics at low temperatures. In this section, we show that the $1/z$ expansion of the RPA free energy converges rapidly above the temperature $T_z \propto Js$. The following section examines the breakdown of the spin-wave approximation above the crossover temperature $\overline{T} \propto zJs > T_z$.

The RPA free energy can be derived by summing the infinite series of ring diagrams shown in Fig. 5, for a hypercubic lattice in d dimensions with $z=2d$ nearest neighbors. Only two spin fluctuations interact at each vertex of every ring diagram. So unlike the exact free energy, the RPA free energy neglects the many-body interactions between more than two spin fluctuations.

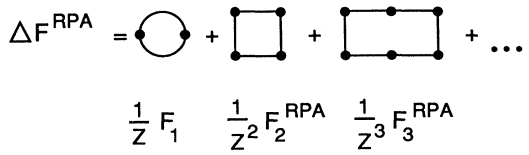

FIG. 5. Diagrammatic representation of the RPA free energy.

Because the disconnected parts of any ring diagram cannot survive, only the fully connected average enters the semi-invariant expansion. According to Eq. (31) for ΔF, the contribution of a ring diagram with n sides is

$$\Delta F_n = -T\frac{(\beta J)^n}{n!}\langle P(R_{i_1 j_1}R_{i_2 j_2}\cdots R_{i_n j_n})\rangle_{\rm MF} , \tag{45}$$

where i_α, j_α label the end points of a bond on the ring. Since R_{ij} commutes with $H_{\rm eff}$, we can define

$$R_{ij}(\tau) \equiv e^{\tau H_{\rm eff}} R_{ij} e^{-\tau H_{\rm eff}} = R_{ij} \tag{46}$$

and we can replace the permutation operator by an integral over a time-ordered product:

$$\Delta F_n = -TJ^n \int_0^\beta d\tau_1 \cdots \int_0^\beta d\tau_n \langle \mathcal{T}_r[R_{i_1 j_1}(\tau_1)\cdots R_{i_n j_n}(\tau_n)]\rangle_{\rm MF} , \tag{47}$$

where $\mathcal{T}_\tau$ is the time-ordering operator.

Since each site index appears exactly twice, the average in Eq. (47) decouples into the product of time-ordered averages for pairs of spins. The correlation functions on any lattice site are defined by

$$\chi^0_{\alpha\gamma}(\tau) = \langle \mathcal{T}_\tau \bar{S}_{1\alpha}(\tau)\bar{S}_{1\gamma}(0)\rangle_{\rm MF} , \tag{48}$$

where α or γ can equal x, y, or z and

$$\bar{S}_{iz} = S_{iz} - M_0 , \tag{49}$$

$$\bar{S}_{ix} = S_{ix} , \tag{50}$$

$$\bar{S}_{iy} = S_{iy} . \tag{51}$$

Because the matrix $\chi^0_{\alpha\gamma}(\tau)$ is a periodic function of τ with period β, its Fourier transform can be defined at discrete Matsubara frequencies:

$$\chi^0_{\alpha\gamma}(\omega_\nu) \equiv \int_0^\beta d\tau \chi^0_{\alpha\gamma}(\tau) e^{-i\omega_\nu \tau} d\tau , \tag{52}$$

$$\omega_\nu = 2\pi\nu T , \tag{53}$$

where ν is an integer. So Eq. (47) can be rewritten as

$$\Delta F_n = -TJ^n \sum_\nu {\rm Tr}[\underline{\chi}^0(\omega_\nu)^n] , \tag{54}$$

where the sum over ν runs from $-\infty$ to ∞.

If the RPA were a simple ring summation, we would multiply Eq. (54) by the total number of ring diagrams of order n:

$$\aleph_n = \frac{1}{2n}\sum{}' \Theta(i_1,i_2)\cdots\Theta(i_{n-1},i_n) , \tag{55}$$

where $\Theta(i,j)=1$ if sites i and j are nearest neighbors and $\Theta(i,j)$ vanishes otherwise. To prevent a ring diagram from crossing itself, we exclude the repetition of any index in the summation of Eq. (55). This is indicated by the prime. The factor of $2n$ appears because every diagram is counted $2n$ times in the summation: any of the n vertices can be the starting point of the ring and each diagram can be traversed in two opposite directions.

But the RPA actually sums over a much larger class of diagrams, which is obtained from the ring diagrams by deforming each ring in all possible ways. For example, the class of RPA "square" diagrams includes a simple square, the two-loop diagram, as well as a diagram with four lines joining neighboring sites. Each of these diagrams is evaluated according to Eq. (54), *as if it were a nonintersecting ring diagram.* The number of RPA "ring" diagrams of order n is

$$\aleph_n^{\rm RPA} = \frac{1}{2n}\sum_{\mathbf{q}} z^n(\gamma_{\mathbf{q}})^n , \tag{56}$$

where

$$\gamma_{\mathbf{q}} = \frac{1}{z}\sum_j e^{i\mathbf{q}\cdot(\mathbf{x}_j - \mathbf{x}_i)}\Theta(i,j) . \tag{57}$$

All momentum sums run over the hypercube $-\pi \leq q_\alpha \leq \pi$ for all α. So we finally obtain the RPA fluctuation free energy

$$\Delta F = -T \sum_{n=1}^{\infty} \sum_{\mathbf{q},\nu} \frac{(zJ)^n}{2n} (\gamma_{\mathbf{q}})^n \mathrm{Tr}[\underline{\chi}^0(\omega_\nu)^n]$$

$$= \frac{T}{2} \sum_{\mathbf{q},\nu} \ln \det[\underline{I} - zJ\gamma_{\mathbf{q}} \underline{\chi}^0(\omega_\nu)] , \tag{58}$$

where $\underline{I}$ is the unit matrix. Because every ring in a hypercubic lattice must have an even number of bonds, the terms with odd n automatically vanish.

The correlation matrix $\underline{\chi}^0(\omega_\nu)$ can be easily evaluated from its definition in Eq. (48). The longitudinal component is

$$\chi^0_{zz}(\omega_\nu) = \beta \delta_{\nu,0} \langle \bar{S}^2_{1z} \rangle_{\mathrm{MF}} , \tag{59}$$

where

$$\langle \bar{S}^2_{1z} \rangle_{\mathrm{MF}} = G_1(T^*) - [M_0(T^*)]^2 . \tag{60}$$

Notice that $zJ\chi^0_{zz}(\omega_\nu = 0)$ is just the function f, defined in Eq. (17). The transverse components are given by

$$\chi^0_{xx}(\omega_\nu) = \chi^0_{yy}(\omega_\nu) = M_0 \frac{\Delta}{\omega_\nu^2 + \Delta^2} , \tag{61}$$

$$\chi^0_{xy}(\omega_\nu) = -\chi^0_{yx}(\omega_\nu) = M_0 \frac{\omega_\nu}{\omega_\nu^2 + \Delta^2} , \tag{62}$$

where $\Delta(T^*) = zJM_0(T^*)$. The mixed terms χ^0_{zx}, χ^0_{xz}, χ^0_{zy}, and χ^0_{yz} all vanish.

Hence, the fluctuation free energy decouples into longitudinal and transverse contributions. For $T < T_C$, we find that

$$\frac{\Delta F_z}{NzJ} = \frac{T^*}{2N} \sum_{\mathbf{q}} \ln(1 - \beta^* \gamma_{\mathbf{q}} \langle \bar{S}^2_{1z} \rangle_{\mathrm{MF}}) , \tag{63}$$

$$\frac{\Delta F_\perp}{NzJ} = \frac{T^*}{N} \sum_{\mathbf{q}} \ln \left[\frac{\sinh(\beta\omega_{\mathbf{q}}/2)}{\sinh(\beta\Delta/2)} \right] , \tag{64}$$

where

$$\omega_{\mathbf{q}} \equiv \Delta(T^*)(1 - \gamma_{\mathbf{q}}) \tag{65}$$

is the RPA spin-wave energy. The exact eigenfrequency of a spin wave with momentum $\mathbf{q}$ is given by Eq. (65) with $\Delta(T^*)$ replaced by zJs. This bare frequency is renormalized by the presence of other spin waves at finite temperatures. For $T > T_C$, ΔF_z is still given by Eq. (63) but $\Delta F_\perp = 2\Delta F_z$.

We have numerically evaluated the RPA fluctuation free energy of Eqs. (63) and (64) by using the density-of-states function

$$D(\gamma) = \frac{1}{N} \sum_{\mathbf{q}} \delta(\gamma - \gamma_{\mathbf{q}}) \tag{66}$$

to transform the momentum integrals into one-dimensional integrals over γ. In the limit $z \to \infty$, $D(\gamma) \to \delta(\gamma)$ and the fluctuation free energy vanishes. Hence, both the longitudinal and transverse free energies can be formally expanded in powers of $\gamma_{\mathbf{q}}$. The nth-order term corresponds to the contribution of the nth-order ring diagram. In a hypercubic lattice,

$$\frac{1}{N} \sum_{\mathbf{q}} (\gamma_{\mathbf{q}})^{2n} = \frac{1}{z^n} \frac{(2n)!}{2^n n!} + O\left[\frac{1}{z^{n+1}} \right] \tag{67}$$

and the contribution of the nth-order ring diagram is of order $1/z^{n/2}$. In particular, the only ring diagram of order $1/z$ is the one-loop diagram. Since any other diagram is at least of order $1/z^2$, *the RPA is exact to order* $1/z$.

Using Eqs. (63) and (64), the first-order free energy can be written as

$$\frac{1}{z} \frac{F_1}{NzJ} = -\frac{\langle \bar{S}^2_{1z} \rangle_{\mathrm{MF}}}{4zT^*} - \frac{M_0^2}{8zT^* \sinh^2(M_0/2T^*)} , \tag{68}$$

where the two terms on the right-hand side are the longitudinal and transverse contributions, respectively. It is straightforward to show that Eq. (68) agrees with Eq. (28) for F_1/NzJ, which was derived in Sec. II.

We have evaluated the RPA specific heat by numerically differentiating the RPA free energy. The results for $s = \frac{3}{2}$ are plotted in the solid lines of Fig. 6. This figure compares the RPA results with the $1/z$ specific heat C_1/N, which is plotted in the dashed lines. Except at low temperatures and near the Curie temperature, the agreement between the RPA and $1/z$ specific heat is quite good.

At low temperatures, the disagreement between the RPA and $1/z$ specific heats is easy to understand. For $T < \Delta$, the transverse RPA free energy may be expanded as

$$\frac{\Delta F_\perp}{N} \approx -T \sum_{n=1}^{\infty} \frac{e^{-n\beta\Delta}}{n} \left[I_0 \left[\frac{2n\beta\Delta}{z} \right]^{z/2} - 1 \right] , \tag{69}$$

where $I_0(x)$ is the zeroth-order Bessel function of imaginary argument.[17] If $T < \Delta/z$, then $I_0(x) \approx e^x/\sqrt{2\pi x}$ for $x \gg 1$. So in three dimensions, Eq. (69) reduces to

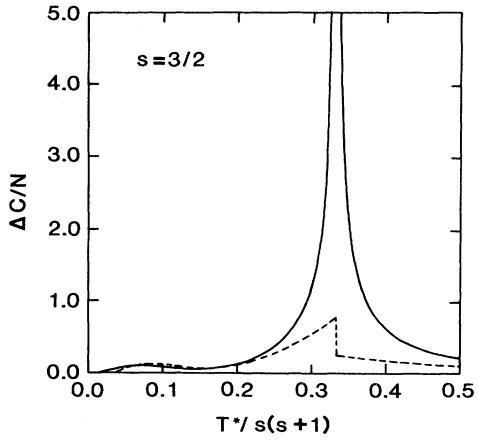

FIG. 6. The RPA fluctuation specific heat $\Delta C^{\mathrm{RPA}}/N$ (solid) and the exact, first-order specific heat C_1/N (dashed) vs $T^*/s(s+1)$ for $s = \frac{3}{2}$.

$$\frac{\Delta F_\perp}{N} \approx -\left[\frac{3}{2\pi}\right]^{3/2} \zeta(\tfrac{5}{2}) \frac{T^{5/2}}{\Delta^{3/2}} . \tag{70}$$

which is the well-known result for the spin-wave free energy. Notice that the power-law behavior of $\Delta F_\perp$ cannot be generated by an expansion of $I_0(x)$ to any finite order in x. Hence, the low-temperature behavior of $\Delta F_\perp$ *cannot be reproduced by a finite expansion in powers of* $1/z$. This explains the discrepancy between the RPA and the $1/z$ specific heats at low temperatures.

The failure of the $1/z$ expansion at low temperatures and near the Curie temperature can also be explained in terms of the momentum summations in Eqs. (63) and (64). Although $\gamma_{\mathbf{q}}$ is formally of order $1/z$ at finite $\mathbf{q}$, it equals 1 for $\mathbf{q}=\mathbf{0}$. At low temperatures, the $\mathbf{q}=\mathbf{0}$ contribution dominates the summation in Eq. (64) for $\Delta F_\perp/N$. Therefore, the $1/z$ expansion of $\Delta F_\perp$ must break down at low temperatures. The $1/z$ expansion also fails near the Curie temperature, where the $\mathbf{q}=\mathbf{0}$ term dominates the summation in Eq. (63) for $\Delta F_z/N$. Because the spin-wave energy vanishes at $\mathbf{q}=\mathbf{0}$, the longitudinal specific heat diverges like $|T-T_C|^{-1/2}$ near T_C. On the other hand, every $1/z$ correction to the specific heat is finite at the MF Curie temperature. Hence, the specific heat of the $1/z$ expansion does not diverge to any finite order.

When $T \geq \Delta/z$, the Bessel function $I_0(x)$ can be approximated[17] by the first few terms of its Taylor expansion in powers of x. This procedure generates a rapidly converging $1/z$ expansion of the transverse free energy. Therefore, we refer to the range of temperatures above $T_z \propto \Delta/z \approx Js$ but not too close to T_C as the $1/z$ regime. Notice that in the limit $z \to \infty$, $T_z^* = T_z/zJ \to 0$ and the RPA free energy tends to its MF limit F_0/NzJ. So for infinite z, the MF free energy can always be represented by its $1/z$ expansion, which is not a surprising result. For finite z, the RPA free energy may be approximated by its $1/z$ expansion above some nonzero temperature $T_z^* \propto s/z$.

By far the most interesting feature of Fig. 6 is the peak in the fluctuation specific heat at the temperature $\bar{T} \approx 0.18zJs$, which lies within the $1/z$ regime. If we assume that $T \ll \Delta$, then the free energy can be approximated by

$$\frac{\Delta F_\perp}{N} \approx -e^{-\beta\Delta} \frac{\Delta^2}{2zT} . \tag{71}$$

This formula cannot be produced by any finite expansion in powers of T. The same result could be obtained by evaluating F_1/NzJ in the limit of small temperature. So in the temperature regime $\Delta/z \leq T \ll \Delta$, the transverse free energy $F_\perp/NzJ$ is well represented by a term of order $1/z$. As shown in the next section, the peak in the fluctuation specific heat can be obtained from this free energy. The peak in C_1/zN is very close to the peak in the full RPA specific heat $\Delta C^{\mathrm{RPA}}/N$, as demonstrated by Fig. 6.

Clearly, the peak can be predicted and explained from the $1/z$ expansion. Yet the peak is also produced by spin-wave contributions to the transverse free energy. As the temperature exceeds the maximum spin-wave energy of order Δ, all spin-wave states contribute to the energy. In this equipartition regime, the transverse free energy becomes a linear function of T and the transverse specific heat vanishes. The transverse specific heat reaches a maximum at the temperature $\bar{T} \approx 0.18\Delta$, where the population of the large momentum spin-wave modes is growing most rapidly. If the spin is large enough that the longitudinal specific heat does not conceal the peak, the total fluctuation specific heat will also peak at $\bar{T}$. In practice, the peak is absent for $s = \frac{1}{2}$ and first appears for $s = 1$.

In the next section, we show that the quantum peak marks the crossover between the linear and nonlinear regimes. Above $\bar{T}$, the spin fluctuations become highly nonlinear and the RPA free energy begins to deviate from the exact free energy, evaluated to order $1/z^2$ in the previous section. The breakdown of the linear description is expected for two reasons. First, the spin-wave theory cannot describe the nonlinear *dynamics* above $\bar{T}$. In the nonlinear regime, the contributions of spin waves with large momenta dominate the RPA free energy. But the interactions between spin waves with large momenta are highly nonlinear and even lead to the formation of bound states. Such nonlinear effects cannot be described by any perturbative scheme which assumes that the single-particle excitations are weakly interacting. Secondly, the *thermodynamic* functions above $\bar{T}$ cannot be represented by a finite expansion in powers of T. Because of the exponential corrections to the free energy, the asymptotic expansion of the free energy fails above $\bar{T}$.

IV. COMPARISON OF THE EXACT AND RPA FREE ENERGIES

In the preceding section the RPA free energy was derived by summing an infinite set of ring diagrams. Since the contribution of a ring diagram with $2n$ lines is proportional to $1/z^n$, the RPA free energy contains terms of every order in $1/z$. In this section, we compare the RPA free energy with the exact free energy evaluated in Sec. II. Above the crossover temperature $\bar{T} \approx 0.18zJs$, the RPA free energy deviates from the exact free energy and the concept of a weakly interacting spin wave loses its meaning.

Like the exact free energy, the RPA free energy can be formally expanded in powers of $1/z$:

$$\frac{F^{\mathrm{RPA}}}{NzJ} = \frac{F_0}{NzJ} + \frac{1}{z}\frac{F_1}{NzJ} + \frac{1}{z^2}\frac{F_2^{\mathrm{RPA}}}{NzJ} + \cdots . \tag{72}$$

As shown in the previous section, this expansion converges rapidly above the temperature $T_z \propto Js$. Each term in the fluctuation free energy $\Delta F^{\mathrm{RPA}} = F^{\mathrm{RPA}} - F_0$ is represented by a ring diagram in Fig. 5. While the first-order correction F_1/NzJ corresponds to the one-loop diagram, the second-order contribution corresponds to the square diagram. The superscript RPA is omitted from the first two terms in Eq. (72) because they agree with the exact results of Sec. II. So the first-order RPA specific heat agrees with C_1/N.

But to order $1/z^2$ and higher, the RPA free energy disagrees with the exact free energy. The square diagram that represents F_2^{RPA}/NzJ is only one of the *infinitely*

many diagrams that represent F_2/NzJ. Because the RPA approximates the number of rings $\aleph_n$ by allowing a ring to intersect itself, the number of square diagrams is counted differently by the RPA and $1/z$ expansions. To leading order in $1/z$, the number of actual square diagrams is $\mathcal{N}_4 = Nz^2/8$ but the number of RPA square diagrams is $\mathcal{N}_4^{\rm RPA} = 3Nz^2/8$. The RPA overcounts the number of square diagrams in order to approximate the contribution of the two-loop diagrams at low temperatures. But the RPA totally neglects the diagrams $F_2^{(b)}/NzJ$ and $F_2^{(m\geq 5)}/NzJ$ which involve three-body interactions between the spins.

Some authors[11,15] have argued that the RPA ring summation is equivalent to an expansion of the free energy to first order in $1/z$. In contrast, we find that the RPA is an uncontrolled expansion to all orders in $1/z$. The fundamental difference between the RPA and $1/z$ expansions is crucial to the following argument, which establishes the limitations of the spin-wave description by comparing the two free energies.

The difference between the RPA and exact free energies, evaluated to order $1/z^2$, is plotted in Fig. 7. The arrows in this figure point to the temperatures $\bar{T} = 0.18zJs$. Obviously, $(F_2^{\rm RPA} - F_2)/NzJ$ becomes significant above a crossover temperature very close to the peak temperature $\bar{T}$. Below $\bar{T}$, the RPA free energy is approximately equal to the exact free energy and the uncontrolled summation of the RPA is justified, at least to order $1/z^2$. In this low-temperature regime, the spin fluctuations of the Heisenberg ferromagnet can be described as spin waves. Above $\bar{T}$, however, the RPA free energy deviates from the exact result and the nonlinear spin fluctuations cannot be described as spin waves. Figure 4 compares the

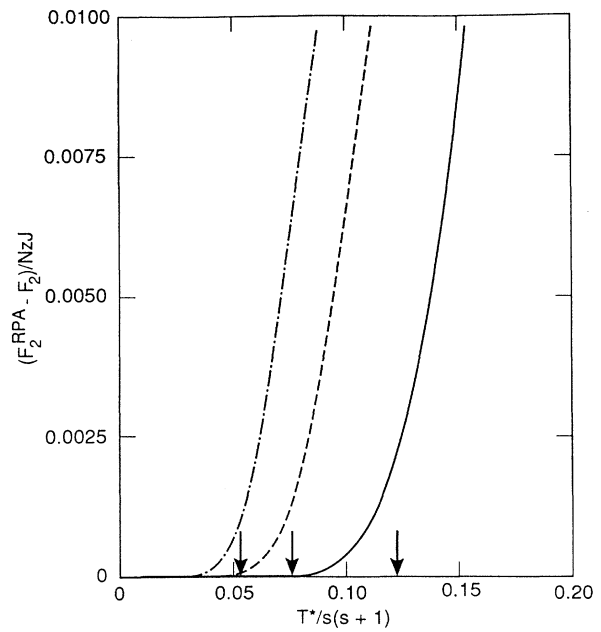

FIG. 7. The difference between the RPA and exact, second-order free energies vs $T^*/s(s+1)$ for $s=\frac{1}{2}$ (solid), $s=\frac{3}{2}$ (dashed), and $s=\frac{5}{2}$ (dot-dashed).

second-order RPA and exact free energies, evaluated with $s=\frac{3}{2}$. For this value of the spin, the crossover temperature is close to $\bar{T}^*/s(s+1)=0.07$.

To study the deviation between F_2 and $F_2^{\rm RPA}$ in a more quantitative manner, we expand the RPA free energy in powers of $y = e^{-\beta\Delta}$. For finite values of the spin,

$$\frac{F_2^{\rm RPA}}{NzJ} = -\tfrac{1}{8}\beta^{*3}s^3y[s+4y(2s-1)]+O(y^3)\ . \tag{73}$$

Comparing this result with Eq. (44) for F_2/NzJ, we find that the lowest-order temperature dependence of both F_2 and $F_2^{\rm RPA}$ is $-\beta^{*3}s^4y/8$. But to order y^2, the two free energies are different. The exact and RPA free energies begin to deviate when this second-order term becomes significant compared with the first-order term. For $s \gg 1$, the difference between the free energies is given by

$$\frac{F_2^{\rm RPA}-F_2}{NzJ} \approx \frac{1}{2}y^2\left[\frac{s}{T^*}\right]^2\left[1-\frac{s}{T^*}+\frac{1}{4}\left[\frac{s}{T^*}\right]^2\right] + O(y^3)\ , \tag{74}$$

which is a function only of T^*/s. Therefore, the free energies will deviate when T^* is of order s or when T is of order zJs. Since the crossover in Fig. 7 occurs very close to the quantum peak at $\bar{T}$, we shall usually not distinguish between the true crossover and the peak temperature. Indeed, as discussed earlier, the appearance of the quantum peak is intimately related to the breakdown of the linear theory.

To summarize these results, we find that for finite values of the spin,

$$\lim_{T^*\to 0}\frac{F_2^{\rm RPA}}{NzJ} = \lim_{T^*\to 0}\frac{F_2}{NzJ} = -\tfrac{1}{8}\beta^{*3}s^4y\ . \tag{75}$$

We expect that the lowest-order temperature dependence of the higher-order corrections $F_{n>2}^{\rm RPA}/NzJ$ also agree with the exact free energy $F_{n>2}/NzJ$. So below the crossover temperature, the RPA free energy is nearly equal to the exact free energy. In that low-temperature regime, the ring summation of the RPA is justified and the spin-wave description is accurate. But above $\bar{T}$, the y^2 terms become significant and the spin-wave approximation fails. In this high-temperature regime, a local description of the spin fluctuations is more appropriate than the long-wavelength description of the RPA.

Because F_2/NzJ is far more complex than $F_2^{\rm RPA}/NzJ$, the agreement in Eq. (75) may be surprising. Below the crossover temperature, however, almost all of the diagrams which contribute to F_2/NzJ are negligible. For example, the contributions of the diagrams $F_2^{(b)}/NzJ$ and $F_2^{(m\geq 5)}/NzJ$ are all proportional to y^2. So below $\bar{T}$, the three-body interactions contained in those diagrams can be neglected. As discussed above, the two-loop diagram involves the simultaneous interaction of four spins. But to linear order in y, this four-body interaction factors into the product of two-body interactions. So below the crossover, the two-loop diagram behaves like a deformed square. When this deformed square is added to the proper square of $F_2^{(a)}/NzJ$, the RPA free energy is recovered.

Above the crossover temperature, however, the three-body interactions are non-negligible and the four-body interaction cannot be treated as the product of two-body interactions. So the spin-wave description breaks down.

Using the results for F_2 and F_2^{RPA}, we have also calculated the second-order specific heats C_2/N and C_2^{RPA}/N, which are plotted in Fig. 8 for $s=\frac{3}{2}$. The difference between the exact and RPA specific heats seems to reach a maximum somewhat below the curie temperature. An unusual feature of Fig. 8 is the appearance of a *second* peak in the fluctuation specific heat. Both C_2 and C_2^{RPA} contain peaks at a temperature $\bar{T}'$, which is well below $\bar{T}$. Like $\bar{T}$, $\bar{T}'$ is also proportional to zJs.

As mentioned in the last section, the peak temperatures can be approximated by retaining only the lowest-order corrections to the fluctuation free energy. Using Eqs. (71) and (75) for the low-temperature limits of the free energies, we obtain the low-temperature limits for the specific heat:

$$\lim_{T^*\to 0}\frac{C_1}{N}=\frac{1}{2}\frac{s^2}{T^{*2}}\left[2-4\frac{s}{T^*}+\frac{s^2}{T^{*2}}\right]e^{-\beta^* s}, \tag{76}$$

$$\lim_{T^*\to 0}\frac{C_2}{N}=\lim_{T^*\to 0}\frac{C_2^{\mathrm{RPA}}}{N}$$

$$=\frac{1}{8}\frac{s^4}{T^{*4}}\left[12-8\frac{s}{T^*}+\frac{s^2}{T^{*2}}\right]e^{-\beta^* s}. \tag{77}$$

These low-temperature results imply that the peaks in C_2/N and C_2^{RPA}/N occur at about the same temperature. Since T^* is always scaled by s, the peak temperatures are proportional to zJs, as expected. Evaluating Eqs. (76) and (77), we find that C_1/N peaks at the temperature $\bar{T}\approx 0.177s$ while C_2/N and C_2^{RPA}/N peak at the lower temperature $\bar{T}'\approx 0.116s$. Hence, the crossover temperature is approximately $0.18zJs$. When the remainder of the specific heat is added to Eqs. (76) and (77), $\bar{T}$ and $\bar{T}'$ are slightly increased.

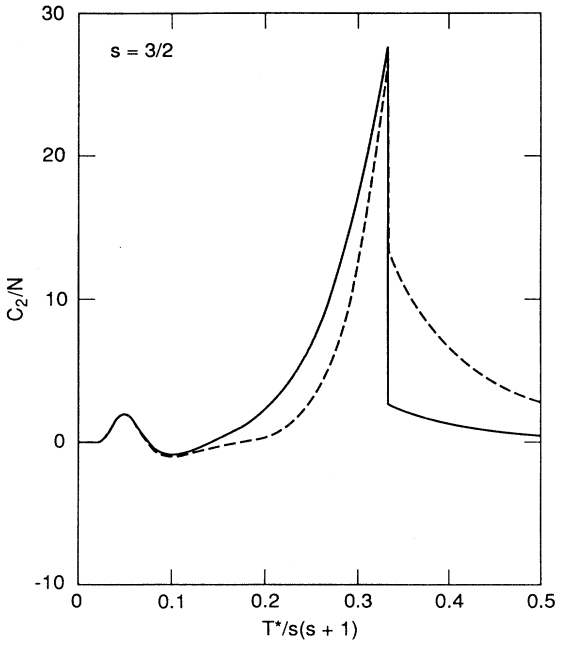

FIG. 8. The second-order specific heat corrections C_2/N (solid) and C_2^{RPA}/N (dashed) vs $T^*/s(s+1)$ for $s=\frac{3}{2}$.

Because the quantum peaks are described by the lowest-order terms in the low-temperature expansions of F_1/NzJ and F_2/NzJ, it seems likely that every fluctuation correction to the specific heat will contain a peak. The peaks in C_n^{RPA}/N and C_n/N can be approximated by retaining only the $e^{-\beta\Delta}$ term in the expansion of Eq. (69) for the transverse free energy. As n increases, the peaks in C_n/N and C_n^{RPA}/N move to lower temperatures. In the limit $n\to\infty$, the peak temperatures vanish.

As shown in the previous section, the peak in C_1/N survives the ring summation to appear in the total RPA fluctuation specific heat $\Delta C^{\mathrm{RPA}}/N$. Because the higher-order peaks in $C_{n>1}^{\mathrm{RPA}}/N$ are below $\bar{T}$, the peak in $\Delta C^{\mathrm{RPA}}/N$ is slightly below the peak in C_1/N. Since the RPA and exact free energies are approximately equal below $\bar{T}$, the peak in C_1/N should also survive the $1/z$ expansion to appear in the total fluctuation specific heat $\Delta C/N$. Like the peak in $\Delta C^{\mathrm{RPA}}/N$, the peak in $\Delta C/N$ will be slightly reduced in temperature but relatively unchanged in height compared with the peak in C_1/N.

Notice that with the temperature scaled by $s(s+1)$, the crossover temperature $\bar{T}/s(s+1)$ vanishes in the classical limit of infinite spin. In units of $T^\dagger=T^*/s(s+1)$, the classical limits of $F_2/NzJs^2$ and C_2/N always disagree with the classical limits of $F_2^{\mathrm{RPA}}/NzJs^2$ and C_2^{RPA}/N, even for very small values of $T^\dagger$. Of course, if the temperature is *not* scaled by $s(s+1)$, then the crossover temperature $\bar{T}\propto zJs$ diverges in the classical limit of infinite spin. This provides the usual justification for a $1/s$ expansion about the noninteracting spin-wave Hamiltonian.[3,9] But for large spin, $T_C/\bar{T}$ scales like s. So the fraction of the magnetic state below $\bar{T}$ *decreases* as the spin increases.

V. CONCLUSION

This paper has described the crossover from a low-temperature spin-wave regime to a high-temperature nonlinear regime in the Heisenberg ferromagnet. We have used the RPA to represent the class of spin-wave theories. The RPA free energy yields the familiar spin-wave thermodynamics when $T\ll\Delta/z$. Although the RPA free energy is exact to order $1/z$, it is only approximate at higher order. Like the $1/z$ specific heat C_1/N, the RPA fluctuation specific heat peaks at the temperature $\bar{T}\approx 0.18zJs$. This peak is created when the transverse free energy enters an equipartition regime in which all momentum states contribute to the energy. Below $\bar{T}$, F_2^{RPA}/NzJ is approximately equal to F_2/N; above $\bar{T}$, the two free energies are substantially different. Therefore, the RPA cannot describe the strongly nonlinear fluctuations above the crossover.

Because *all* the many-body interactions are significant above $\bar{T}$, the RPA cannot be repaired by simply adding a finite set of nonlinear terms to the spin-wave Hamiltonian. For example, suppose that the three- and four-body interactions are added to the spin-wave Hamiltonian.

Even if the spin-wave free energy could be evaluated *exactly,* it would still exclude the five- and six-body interactions which contribute to F_3/NzJ above $\bar{T}$. Although the spin-wave theory may be very accurate at low temperatures when $y \approx e^{-\beta^* s}$ is small, it will necessarily fail above a crossover temperature of order zJs when y is of order 1 and the many-body interactions are important. In practice, the $1/z$ expansion is the only method which can be used to study the thermodynamics of a ferromagnet above $\bar{T}$.

The breakdown of the spin-wave description is closely related to the appearance of the quantum peak at $\bar{T}$. Above the quantum peak, the large-momentum spin waves dominate the free energy and the many-body interactions must be retained. Because these nonlinear effects violate the assumptions of the spin-wave picture, the concept of a spin wave loses its meaning above $\bar{T}$.

The appropriate expansion parameters are different on either side of the crossover. Below $\bar{T}$, the $1/z$ expansion converges rather slowly. In fact, the free energy at low temperatures is a nonanalytic function of $1/z$. Each term in the $1/z$ expansion of the RPA free energy is exact to linear order in y. Summing these linear terms produces the power-law behavior of the free energy. Hence, the appropriate expansion parameter at low temperatures is y and not $1/z$. But above the crossover, y is of order 1 and each $1/z$ correction to the free energy is a slowly converging function of y. Instead of y, $1/z$ becomes the controlling parameter.

We believe that the results of this paper are independent of the specific model we have used to calculate the crossover temperature. As just discussed, the crossover temperature does not change if the RPA is replaced by a more sophisticated spin-wave theory. In order to calculate the second-order corrections F_2/NzJ and F_2^{RPA}/NzJ, we have chosen to work on a hypercubic lattice. But the temperature of the quantum peak in C_1/N does not depend on the lattice topology. Therefore, the crossover temperature should be near $0.18zJs$ for any three-dimensional lattice.

Thermodynamically, the crossover appears in the peak of the *fluctuation* specific heat. Unfortunately, as shown in Figs. 9 and 10 for a cubic lattice, this peak does not appear in the *total* specific heat. While the solid lines are the RPA specific heat, the dashed lines are the expansion $C = C_0 + C_1/z$. In the figures for both C/N and $C/NT^{\dagger}$, the quantum peak is concealed by the large MF specific heat C_0/N. To uncover the quantum peak, the MF specific heat must be subtracted from the data. Since C_0/N is a function only of $T^* = T/zJ$ and of s, this subtraction should be straightforward.

Although the crossover does not appear as a peak, it *does* appear as a shoulder in the total specific heat. As mentioned in Sec. II, the exponential term e^{-s/T^*} is responsible for both the shoulder in C_0/N and the peak in C_1/N. Hence, the shoulder in the total specific heat occurs near the crossover temperature $\bar{T}$. This feature is enhanced when the specific heat is divided by the temperature. Numerically, we find that when $s \geq 3$, $C/NT^{\dagger}$ contains a peak near $\bar{T}$. As shown in Fig. 10 for $s = \frac{3}{2}$, the shoulder in $C/NT^{\dagger}$ nearly coincides with the quantum peak at $\bar{T}^{\dagger} = 0.071$.

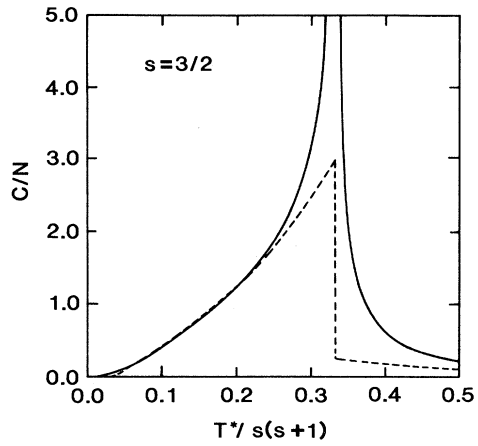

FIG. 9. The total RPA specific heat C^{RPA}/N (solid) and the $1/z$ specific heat $C_0/N + C_1/Nz$ (dashed) vs $T^*/s(s+1)$ for $s = \frac{3}{2}$ and $z = 6$.

This shoulder has been observed in the specific heat of gadolinium[18] (with spin $\frac{7}{2}$) and terbium[19] (with spin 6). Our theory predicts a crossover temperature of about T_C/s, in good agreement with the locations of the shoulders in the experimental data. For terbium, the peak in C/NT appears at a temperature $T/T_C \approx 0.18$, in excellent agreement with our prediction of $1/s = 0.17$. We are hopeful that other measurements of the specific heat will also support our theory for the nonlinear crossover.

Recently, Gros and Johnson[20] have developed a $1/z$ expansion for the mode frequencies of a spin-$\frac{1}{2}$ antiferromagnet at zero temperature. Using a related approach, we have evaluated the mode frequencies in a ferromagnet above $\bar{T}$ to first order in $1/z$. To zeroth order in $1/z$, the mode frequencies are identical to the RPA frequencies ω_q. So above $\bar{T}$, *the nonlinear mode frequencies are very close to the RPA spin-wave frequencies.* Observing this

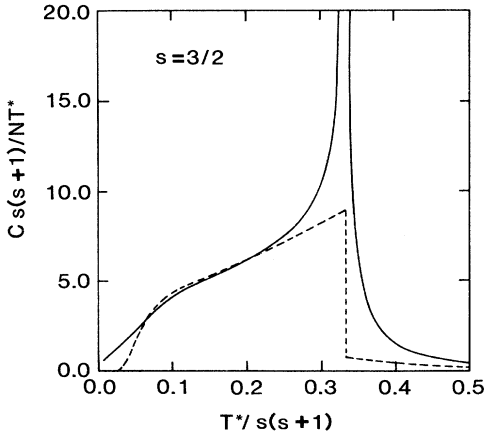

FIG. 10. The total RPA specific heat $C^{\mathrm{RPA}} s(s+1)/NT^*$ (solid) and the $1/z$ specific heat $(C_0 + C_1/z)s(s+1)/NT^*$ (dashed) vs $T^*/s(s+1)$ for $s = \frac{3}{2}$ and $z = 6$.

agreement, some experimentalists[21,22] have claimed that spin waves are well defined up to temperatures very close to T_C. Although their frequencies are indeed close to the RPA frequencies, the nonlinear modes must not be interpreted as spin-wave excitations. Because the $1/z$ corrections to the nonlinear mode frequencies differ from the lowest-order corrections to the spin-wave frequencies, the crossover may be observable in neutron-scattering experiments. Details of this work will be reported in a separate paper.

The calculations presented in this paper clearly demonstrate the importance of nonlinear effects above $\overline{T}$. Very little is presently known about the nonlinear regime between $\overline{T}$ and T_C. In the future, we hope to develop the same sort of intuition for the nonlinear modes above $\overline{T}$ as presently exists for the spin waves below $\overline{T}$.

ACKNOWLEDGMENTS

We would like to acknowledge useful conversations with Dr. J. Fernandez-Baca, Dr. C. Gros, D. M. Johnson, Dr. S. H. Liu, and Dr. T. Kaplan. One of us (R.S.F.) would like to acknowledge support from the U.S. Department of Energy (USDOE) under Contract No. DE-AC05-84OR21400 with Martin Mareitta Energy Systems, Inc. and from the National Science Foundation (NSF) Grant No. DMR-8704210.

APPENDIX A

This appendix generalizes the work of Horwitz and Callen[14] to derive the semi-invariant expansion for the fluctuation free energy of the Heisenberg model. Horwitz and Callen used such an expansion to obtain the fluctuation free energy of the Ising model, in which all the operators commute. The semi-invariant expansion is derived in terms of the function

$$\phi(a)=\ln\langle e^{ax}\rangle=\ln \mathrm{Tr}[e^{ax}\rho(x)] , \tag{A1}$$

where $\rho(x)$ is any normalized weighting factor such as a density matrix. Notice that $\phi(a)$ can be rewritten as

$$\phi(a)=\lim_{\alpha\to 0} e^{aD_\alpha}\ln \mathrm{Tr}[\rho_\alpha(x)] , \tag{A2}$$

where

$$D_\alpha=\frac{\partial}{\partial\alpha} , \tag{A3}$$

$$\rho_\alpha(x)=e^{\alpha x}\rho(x) . \tag{A4}$$

Expanding the exponent of the derivative yields the required semi-invariant expansion

$$\phi(a)=\sum_{n=1}^{\infty}\frac{a^n}{n!}M_n(x) , \tag{A5}$$

where the nth-order semi-invariant is defined by

$$M_n(x)=\lim_{\alpha\to 0} D_\alpha^n \ln \mathrm{Tr}[\rho_\alpha(x)] . \tag{A6}$$

The first few semi-invariants are

$$M_1(x)=\langle x\rangle , \tag{A7}$$

$$M_2(x)=\langle x^2\rangle-\langle x\rangle^2 , \tag{A8}$$

$$M_3(x)=\langle x^3\rangle-3\langle x^2\rangle\langle x\rangle+2\langle x\rangle^3 , \tag{A9}$$

where the $\alpha\to 0$ limit has been performed.

For either the Heisenberg or Ising models, the fluctuation free energy is given in terms of the fluctuation energy H_2 by

$$\Delta F=-T\ln\langle e^{-\beta H_2}\rangle_{\mathrm{MF}} , \tag{A10}$$

which is evaluated with the MF density matrix ρ_0. Comparing Eqs. (A10) and (A1), we find that

$$\Delta F=-T\sum_{n=1}^{\infty}M_n(-H_2) . \tag{A11}$$

For the Heisenberg model, the fluctuation energy is defined by

$$-H_2=J\sum_{\langle ij\rangle}R_{ij} , \tag{A12}$$

where the R_{ij} *do not* commute. Because R_{ij} does commute with H_{eff}, we can define as in Sec. III,

$$R_{ij}(\tau)\equiv e^{\tau H_{\mathrm{eff}}}R_{ij}e^{-\tau H_{\mathrm{eff}}}=R_{ij} . \tag{A13}$$

In the following, these operators will be used to remove the ambiguities associated with the noncommutation of the R_{ij}.

The semi-invariant can now be written as

$$M_n(-H_2)=\lim_{\{\alpha\}\to 0}J^n\left[\sum_{\langle ij\rangle}D_{ij}\right]^n\ln \mathrm{Tr}\rho_{\{\alpha\}} , \tag{A14}$$

where we have introduced a set of $Nz/2$ variables α_{ij} and defined the differential functions D_{ij} and the generalized density matrix $\rho_{\{\alpha\}}$:

$$D_{ij}=\frac{\partial}{\partial\alpha_{ij}} , \tag{A15}$$

$$\rho_{\{\alpha\}}=\rho_0\overline{T}_\tau\exp\left[\sum_{\langle ij\rangle}\int_0^{\alpha_{ij}}R_{ij}(\tau)d\tau\right] , \tag{A16}$$

where $\overline{T}_\tau$ is the anti-time-ordering operator. We have defined $\rho_{\{\alpha\}}$ so that

$$D_{ij}\rho_{\{\alpha\}}=\rho_{\{\alpha\}}R_{ij} \tag{A17}$$

with R_{ij} acting to the right. If the generalized nth-order semi-invariant is defined by

$$M^{(n)}_{\{ij\}}=\lim_{\{\alpha\to 0\}}D_{i_1j_1}D_{i_2j_2}\cdots D_{i_nj_n}\ln \mathrm{Tr}\rho_{\{\alpha\}} , \tag{A18}$$

then the fluctuation free energy can finally be written as

$$\Delta F=-T\sum_{n=1}^{\infty}\frac{(\beta J)^n}{n!}\prod_{m=1}^{n}\sum_{\langle i_m,j_m\rangle}M^{(n)}_{\{i_1,j_1;\ldots;i_n,j_n\}} , \tag{A19}$$

which is the semi-invariant expansion for the Heisenberg model.

APPENDIX B

In this appendix, we summarize the results for the fluctuation free energies. As derived in FL, the first-order free energy F_1/NzJ is given by

$$\frac{F_1}{NzJ}=-\tfrac{1}{4}\beta^{*3}\{(M_0^2-G_1)^2+\tfrac{1}{2}[G_1-s(s+1)]^2-\tfrac{1}{2}M_0^2\}\ , \tag{B1}$$

where $G_1(T^*)$ were defined by Eq. (31). Note that this correction is the same for the RPA and the $1/z$ expansion.

The second-order RPA correction $F_2^{\rm RPA}/NzJ$ is also rather simple. We find that

$$\frac{F_2^{\rm RPA}}{NzJ}=-\frac{\beta^{*3}}{64}\{24(G_1-M_0^2)^4+M_0^4+3[G_1-s(s+1)]^4 -4M_0^2[G_1-s(s+1)]^2\}\ , \tag{B2}$$

which also only depends on $M_0(T^*)$ and $G_1(T^*)$.

For the second-order, exact correction F_2/NzJ, it is more convenient to provide expressions for each of the MF expectation values that enter the components Q_1 and Q_2 of Eqs. (22) and (23). The interested reader can add everything together to obtain the total correction:

$$\langle R_{12}^2\rangle_{\rm MF}=(M_0^2-G_1)^2+\tfrac{1}{2}[G_1-s(s+1)]^2-\tfrac{1}{2}M_0^2\ , \tag{B3}$$

$$\langle R_{12}^3\rangle_{\rm MF}=(G_2-2M_0G_1+2M_0^3)^2+(G_1M_0-G_2)^2 +\tfrac{1}{2}(G_1M_0-M_0-G_2)^2-(G_1-M_0^2)^2-2[G_1-\tfrac{1}{2}s(s+1)-\tfrac{1}{2}M_0^2]^2\ , \tag{B4}$$

$$\langle P(R_{12}R_{23}R_{34}R_{41})\rangle_{\rm MF}=24(G_1-M_0^2)^4+M_0^4+3[G_1-s(s+1)]^4-4M_0^2[G_1-s(s+1)]^2\ , \tag{B5}$$

$$\begin{aligned}\langle P(R_{12}^2R_{23}^2)\rangle_{\rm MF}=&\ 6(G_1-M_0^2)^2(G_3-4M_0G_2+6M_0^2G_1-3M_0^4)\\ &+(G_1-M_0^2)[G_1-s(s+1)][-6G_3+12M_0G_2-6M_0^2G_1\\ &\qquad +6s(s+1)(G_1-M_0^2)-5G_1+4M_0^2+s(s+1)]\\ &+\tfrac{1}{2}[G_1-s(s+1)]^2[3s^2(s+1)^2-6s(s+1)G_1+3G_3+5G_1-2s(s+1)]\\ &-M_0(G_1-M_0^2)(10G_2-16M_0G_1+6M_0^3+M_0)+2M_0^2G_1\\ &+[G_1-s(s+1)]M_0[5s(s+1)M_0-5G_2-M_0]\ ,\end{aligned} \tag{B6}$$

$$\langle R_{12}^2(S_{1z}-M_0)\rangle_{\rm MF}=-2M_0^5+\tfrac{1}{2}M_0^3(1+10G_1)-M_0^2G_2+\tfrac{1}{2}M_0G_1[s(s+1)-1-7G_1]-\tfrac{1}{2}G_2s(s+1)+\tfrac{3}{2}G_1G_2\ . \tag{B7}$$

Notice that each expectation value vanishes at $T^*=0$.

APPENDIX C

In this appendix, we show that the free energy and entropy

$$\frac{S}{N}=-\frac{d}{dT^*}\frac{F}{NzJ} \tag{C1}$$

are continuous at the Curie temperature. The $1/z$ expansion of the entropy is formally given by

$$S=S_0(T^*)+\frac{1}{z}S_1(T^*)+\frac{1}{z^2}S_2(T^*)+\cdots\ , \tag{C2}$$

where the components of the entropy are related to the free energy corrections by

$$\frac{S_n}{N}=-\frac{d}{dT^*}\frac{F_n}{NzJ}\ , \tag{C3}$$

for all n.

The change in entropy at the Curie temperature is

$$\begin{aligned}\delta S&=\lim_{\epsilon\to 0+}\{S(T_C^*+\epsilon)-S(T_C^*-\epsilon)\}\\ &=\lim_{\epsilon\to 0+}[S(T_0+(1/z)T_1+\cdots+\epsilon)\\ &\qquad -S(T_0+(1/z)T_1+\cdots-\epsilon)]\ .\end{aligned} \tag{C4}$$

We expand δS in powers of $1/z$ as

$$\delta S=\delta s_0+\frac{1}{z}\delta s_1+\frac{1}{z^2}\delta s_2+\cdots\ . \tag{C5}$$

Because the MF entropy is continuous at T_0

$$\delta s_0=\lim_{\epsilon\to 0}[S_0(T_0+\epsilon)-S_0(T_0-\epsilon)]=0\ . \tag{C6}$$

To order $1/z$,

$$\begin{aligned}\delta s_1=&\ T_1\lim_{\epsilon\to 0+}\left[\frac{dS_0}{dT^*}\bigg|_{T_0+\epsilon}-\frac{dS_0}{dT^*}\bigg|_{T_0-\epsilon}\right]\\ &+\lim_{\epsilon\to 0+}[S_1(T_0+\epsilon)-S_1(T_0-\epsilon)]\ .\end{aligned} \tag{C7}$$

Notice that the first-order change in the entropy at T_C^* contains an extra term due to the shift in T_C^* from T_0.

In order to evaluate δs_1, we use the MF relation

$$C_0 = T^* \frac{dS_0}{dT^*} \ . \tag{C8}$$

Hence,

$$\frac{1}{N}\lim_{\epsilon\to 0+}\left[\left.\frac{dS_0}{dT^*}\right|_{T_0+\epsilon} - \left.\frac{dS_0}{dT^*}\right|_{T_0-\epsilon}\right] = \frac{1}{T_0}\lim_{\epsilon\to 0+}\left[\frac{C_0(T_0+\epsilon)}{N} - \frac{C_0(T_0-\epsilon)}{N}\right] = -\frac{15}{2s(s+1)+1} \ , \tag{C9}$$

which uses the MF result for the specific heat jump at T_0. Since the first-order correction to T_0 is

$$T_1 = -\tfrac{1}{3}s(s+1) - \tfrac{1}{4} \ , \tag{C10}$$

we are done with the first term in δs_1.

To obtain the second term, we must calculate the first-order entropy S_1 above and below T_0. Therefore, we require the first-order free energy F_1/NzJ near the MF Curie temperature. Using Eq. (B1), we find

$$\frac{1}{N}\lim_{\epsilon\to 0+} S_1(T_0+\epsilon) = -\tfrac{3}{4} \ , \tag{C11}$$

$$\frac{1}{N}\lim_{\epsilon\to 0+} S_1(T_0-\epsilon) = \frac{7s(s+1)+6}{4s(s+1)+2} \ . \tag{C12}$$

So the second term is given by

$$\frac{1}{N}\lim_{\epsilon\to 0+}[S_1(T_0+\epsilon)-S_1(T_0-\epsilon)] = -\frac{20s(s+1)+15}{8s(s+1)+4} \tag{C13}$$

and the first-order change in entropy at T_C^* is

$$\delta s_1 = 0 \ , \tag{C14}$$

as expected. The derivation of δs_2 would require T_2, which is not yet available.

It is also straightforward to show that the free energy is continuous at the true, shifted Curie temperature. The change in free energy at T_C^* is

$$\delta F = \lim_{\epsilon\to 0+}\{F(T_C^*+\epsilon)-F(T_C^*-\epsilon)\} = \lim_{\epsilon\to 0+}[F(T_0+(1/z)T_1+\cdots+\epsilon) - F(T_0+(1/z)T_1+\cdots-\epsilon)] \ . \tag{C15}$$

As usual, we expand δF in powers of $1/z$ as

$$\delta F = \delta f_0 + \frac{1}{z}\delta f_1 + \frac{1}{z^2}\delta f_2 + \cdots \ . \tag{C16}$$

Because the MF free energy is continuous at T_0,

$$\delta f_0 = \lim_{\epsilon\to 0}[F_0(T_0+\epsilon)-F_0(T_0-\epsilon)] = 0 \ . \tag{C17}$$

To order $1/z$,

$$\delta f_1 = T_1 \lim_{\epsilon\to 0+}\left[\left.\frac{dF_0}{dT^*}\right|_{T_0+\epsilon} - \left.\frac{dF_0}{dT^*}\right|_{T_0-\epsilon}\right] + \lim_{\epsilon\to 0+}[F_1(T_0+\epsilon)-F_1(T_0-\epsilon)] = 0 \ , \tag{C18}$$

because F_1 is also continuous at T_0.

The second-order change in the free energy is given by

$$\delta f_2 = T_2 \lim_{\epsilon\to 0+}\left[\left.\frac{dF_0}{dT^*}\right|_{T_0+\epsilon} - \left.\frac{dF_0}{dT^*}\right|_{T_0-\epsilon}\right] + \frac{1}{2}T_1^2 \lim_{\epsilon\to 0+}\left[\left.\frac{d^2F_0}{dT^{*2}}\right|_{T_0+\epsilon} - \left.\frac{d^2F_0}{dT^{*2}}\right|_{T_0-\epsilon}\right] + T_1 \lim_{\epsilon\to 0+}\left[\left.\frac{dF_1}{dT^*}\right|_{T_0+\epsilon} - \left.\frac{dF_1}{dT^*}\right|_{T_0-\epsilon}\right] + \lim_{\epsilon\to 0+}[F_2(T_0+\epsilon)-F_2(T_0-\epsilon)] = 0 \ . \tag{C19}$$

Notice that the first term, proportional to T_2, vanishes because S_0 is continuous at T_0. Hence, T_2 does not enter δf_2. Using Eq. (C18) and the definition of the specific heat in Eq. (C8), we find that

$$\frac{\delta f_2}{NzJ} = +\frac{1}{2}\frac{T_1^2}{T_0}\lim_{\epsilon\to 0+}\left[\left.\frac{C_0}{N}\right|_{T_0+\epsilon} - \left.\frac{C_0}{N}\right|_{T_0-\epsilon}\right] + \lim_{\epsilon\to 0+}\left[\left.\frac{F_2}{NzJ}\right|_{T_0+\epsilon} - \left.\frac{F_2}{NzJ}\right|_{T_0-\epsilon}\right] \ . \tag{C20}$$

Since the MF specific heat jump is not zero, Eq. (C19) implies that *F_2/NzJ must be discontinuous at T_0 in order for the total free energy to be continuous at T_C^**. Because the RPA free energy is continuous at T_0, it is inconsistent to order $1/z^2$.

To demonstrate the continuity of the free energy, we use the limit

$$\lim_{T^*\to T_0}\frac{(M_1^{(2)})^2}{1-f} = \frac{5}{48}\frac{[4s(s+1)+3]^2}{2s(s+1)+1} \ , \tag{C21}$$

which is easy to derive from the definitions of $M_1^{(2)}$ and f. From Eq. (29), we find that the discontinuity in F_2/NzJ equals half of this result. Substituting in Eq. (C9) for the MF jump in the specific heat, we finally obtain

$$\delta f_2 = 0 \ , \tag{C22}$$

as expected. Hence, the discontinuity in F_2/NzJ is precisely the amount required to produce a continuous free energy.

APPENDIX D

In this appendix, we show how the RPA can be derived from an elementary treatment of the linear response about the MF state. We introduce the Hamiltonian

$$H(\lambda) = H_{\text{eff}} + H_1 + \lambda H_2 \ , \tag{D1}$$

which reduces to the Heisenberg ferromagnet when $\lambda = 1$ and to the MF Hamiltonian when $\lambda = 0$. According to the Hellmann-Feynman theorem

$$\frac{dF(\lambda)}{d\lambda} = \langle H_2 \rangle_\lambda \ , \tag{D2}$$

where the average is taken in the canonical ensemble of $H(\lambda)$.

Integrating Eq. (D2), we obtain the free energy at $\lambda=1$:

$$F=F_0+\int_0^1 d\lambda\langle H_2\rangle_\lambda \ , \tag{D3}$$

or

$$\Delta F=-J\sum_{\langle i,j\rangle}\sum_{\alpha}\int_0^1 d\lambda\langle \bar{S}_{i\alpha}\bar{S}_{j\alpha}\rangle_\lambda$$
$$=-\frac{JzT}{2}\sum_{\mathbf{q},\nu}\int_0^1 d\lambda\,\mathrm{Tr}[\underline{\chi}^\lambda(\mathbf{q},\omega_\nu)]\gamma_{\mathbf{q}} \ . \tag{D4}$$

Here we have used the well-known result of linear-response theory,

$$\{\underline{\chi}^\lambda_{ij}(\tau)\}_{\alpha\gamma}=\langle \mathcal{T}_\tau \bar{S}_{i\alpha}(\tau)\bar{S}_{j\gamma}(0)\rangle_\lambda \ , \tag{D5}$$

which is the time-ordered linear-response function at coupling constant λ.

While Eq. (D4) is an exact expression for the fluctuation free energy, the RPA can be viewed as a simple approximation for $\underline{\chi}^\lambda(\mathbf{q},\omega)$. Apply an external field $h_\alpha(\mathbf{q},\omega)$, which couples linearly to the spin fluctuations $\bar{S}_\alpha(\mathbf{q},\omega)$. The RPA assumes that the system responds with the MF response function $\underline{\chi}^0(\mathbf{q},\omega)$ to an *effective* field given by

$$h^{\mathrm{eff}}_\alpha(\mathbf{q},\omega)=h_\alpha(\mathbf{q},\omega)+\lambda zJ\gamma_{\mathbf{q}}\bar{S}_\alpha(\mathbf{q},\omega) \ , \tag{D6}$$

where

$$\bar{S}_\alpha(\mathbf{q},\omega)=\sum_\gamma \chi^\lambda_{\alpha\gamma}(\mathbf{q},\omega)h_\gamma(\mathbf{q},\omega)=\sum_\gamma \chi^0_{\alpha\gamma}h^{\mathrm{eff}}_\gamma(\mathbf{q},\omega) \tag{D7}$$

is the self-consistent response at coupling constant λ.

Finally, combining Eq. (D6) and (D7), we obtain

$$\underline{\chi}^\lambda(\mathbf{q},\omega)=\underline{\chi}^0(\mathbf{q},\omega)[\underline{I}-\lambda zJ\gamma_{\mathbf{q}}\underline{\chi}^0(\mathbf{q},\omega)]^{-1} \ . \tag{D8}$$

Putting this into Eq. (D4) and evaluating the λ integral, we obtain

$$\Delta F=\frac{T}{2}\sum_{\mathbf{q},\nu}\mathrm{Tr}\ln[\underline{I}-zJ\underline{\chi}^0(\mathbf{q},\omega_\nu)] \ , \tag{D9}$$

which reduces to Eq. (61) in the text.

---

*Permanent address.

[1]See, for example, R. M. White, *Quantum Theory of Magnetism* (Springer-Verlag, Berlin, 1963); or D. C. Mattis, *The Theory of Magnetism I* (Springer, Berlin, 1988), Chap. 5.

[2]F. J. Dyson, Phys. Rev. **102**, 1217 (1956).

[3]T. Oguchi, Phys. Rev. **117**, 117 (1960).

[4]M. Wortis, Phys. Rev. **132**, 85 (1963); **138**, A1126 (1965).

[5]V. G. Vaks, A. I. Larkin, and S. A. Pikin, Zh. Eksp. Teor. Fiz. **53**, 281 (1967) [Sov. Phys. JETP **26**, 188 (1968)]; **53**, 1089 (1967) [**26**, 647 (1968)].

[6]W. Marshall and G. Murray, J. Appl. Phys. **39**, 380 (1968); J. Phys. C **2**, 539 (1969).

[7]R. H. Parmenter, Phys. Rev. B **30**, 2745 (1984).

[8]R. S. Fishman and S. H. Liu, Phys. Rev. B **40**, 11 028 (1989).

[9]T. Holstein and H. Primakoff, Phys. Rev. **58**, 1048 (1940).

[10]F. Englert, Phys. Rev. Lett. **5**, 102 (1960).

[11]R. B. Stinchcombe, G. Horwitz, F. Englert, and R. Brout, Phys. Rev. **130**, 155 (1963).

[12]R. S. Fishman, Phys. Rev. B **41**, 4377 (1990).

[13]R. S. Fishman and G. Vignale (unpublished).

[14]G. Horwitz and H. B. Callen, Phys. Rev. **124**, 1757 (1961).

[15]R. Brout, in *Magnetism*, edited by G. T. Rado and H. Suhl (Academic, New York, 1965), Vol. 2A, p. 43.

[16]See, for example, G. D. Mahan, *Many-Particle Physics* (Plenum, New York, 1981), Chap. 3.

[17]See, for example, *Handbook of Mathematical Functions*, edited by M. Abramowitz and I. A. Stegun (National Bureau of Standards, Washington, 1972), Chap. 9.

[18]M. Griffel, R. E. Skochdopole, and F. H. Spedding, Phys. Rev. **93**, 657 (1954).

[19]L. D. Jennings, R. M. Stanton, and F. H. Spedding, J. Chem. Phys. **27**, 909 (1957).

[20]Claudius Gros and M. D. Johnson, Phys. Rev. B **40**, 9423 (1989).

[21]O. W. Dietrich, J. Als-Nielsen, L. Passell, Phys. Rev. B **14**, 4923 (1976).

[22]H. G. Bohn, A. Kollmar, and W. Zinn, Phys. Rev. B **30**, 6504 (1984).